IOSR Journal of Mechanical and Civil Engineering (IOSR-JMCE)
e- ISSN: 2278-1684, p-ISSN : 2320–334X
PP 66-73
www.iosrjournals.org

NUMERICAL SIMULATION OF COMBUTION CHAMBER GEOMETRY ON A H.S.D.I. DIESEL ENGINE – A CFD APPROACH

P. Vijayakumaran[1], R.Elayaraja[2], A. Muthuvel[3], Dr. M.Subramanian[4] , Rajesh Murukesan[5]

[1*2*3]*(Department of Automobile Engineering, Hindustan University, India)*
[4*5]*(Department of Automobile Engineering, KVCET, India)*

ABSTRACT: *Due to the stringent legislation on emissions from diesel engines and also increasing demand on fuel consumption, the importance of detailed 3D simulation of fuel injection, mixing and combustion has been increased in the recent years. The Common-rail injection system has allowed achieving a more flexible fuel injection Control in DI-diesel engines by permitting a free mapping of the start of injection, Injection pressure, rate of injection. All these benefits have to be gain by installing this device in combustion chambers born to work with the conventional distributor and in-line-pump injection systems. Their design was aimed to improve air-fuel mixing and therefore they were characterized by the adoption re-entrant bowls.*

All the other relevant parameters namely compression ratio, maximum diameter of the bowl, squish clearance and injection rate were kept constant. A commercial CFD code STAR-CD was used to model the in-cylinder flows and combustion process, and experimental results of the baseline bowl have been used to validate the numerical models. The simulation results show that, bowl 3 enhance the turbulence and hence results in better air-fuel mixing among all three bowls in a DI diesel engine. As a result, the ISFC and soot emission reduced, although the NO_X emission is increased owing to better mixing and a faster combustion process.

Key word **-** Combustion chamber, CFD analysis, Fuel consumption.

I. INTRODUCTION

Any physical fluid flow problem can be solved either experimentally or numerically. The numerical simulation is more suitable for parametric studies and it also gives accurate results by solving governing equations in each and every cell of the fluid domain. In the recent years there were tremendous improvement in the field of numerical techniques, which made a great impact on the evaluation of complex flow problems and achieving their solution.

In the present work a three dimensional numerical simulation of the in-cylinder process of a four stroke direct injection diesel engine has been done using commercially available CFD software named STAR-CD. Since the work is focused on swirl velocity component at the end of compression, instead of modeling all the four strokes of the piston, only compression stroke is simulated for two re-entrant bowls and a toroidal bowl. Hence BDC position is taken as starting point for the piston movement (BDC assumes a CA as 0˚).

THE MAIN GOALS TO BE ACHIEVED BY NEWER DIESEL ENGINES INCLUDE THE FOLLOWING:

- Simultaneous reduction in NOX and particulate emissions.
- Optimization of fuel economy.
- Reduction in heat losses during and after combustion.
- Reduction in engine noise and vibration.
- Reduction in engine component weight.
- Flow optimization inside the combustion chamber.

II. PHYSICAL MODEL

The engine studied in this work is a stationary, single-cylinder direct-injection Diesel engine with three different piston shapes were considered. These shapes are representative of the geometries usually employed for the optimum combustion process in real engines. The piston named Model A has a toroidal chamber and used as a baseline model. Piston named Model B is a weakly re-entrant chamber with central projection. The piston

named Model C is a largely reentrant geometry are shown in Figs. from1-3.The engine specifications are given in the Table1.

Table 1 Engine specifications

Number of cylinders	One
Bore	102 mm
Stroke	116 mm
Connecting rod length	174 mm
Compression ratio	16.3:1
Engine speed	1500 rpm
Power	10 bhp
Spray angle (from cylinder head)	25˚
Injection pressure	200 bar
Swirl ratio	2.2 at BDC
Number of holes	3

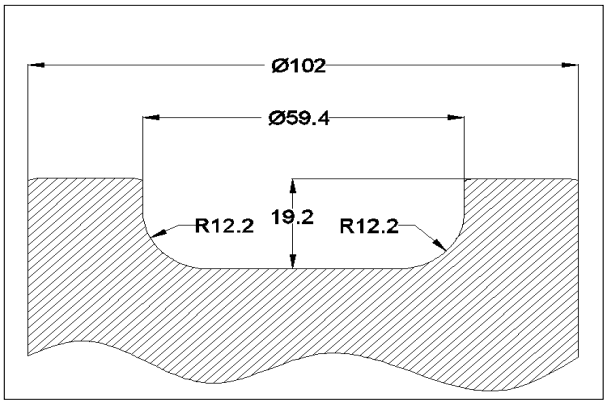

Fig.1 Model -A: View of combustion chamber

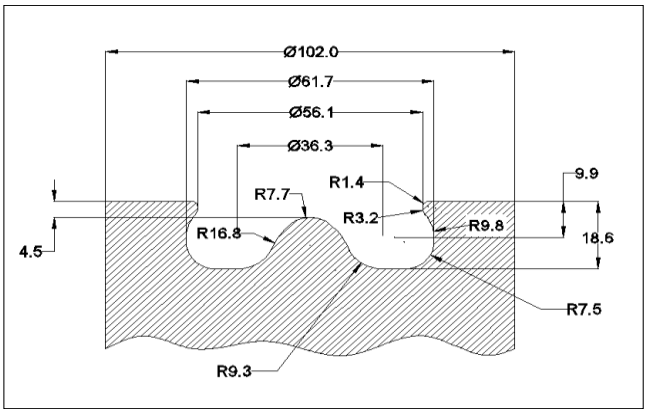

Fig. 2 Model -B: View of combustion chamber

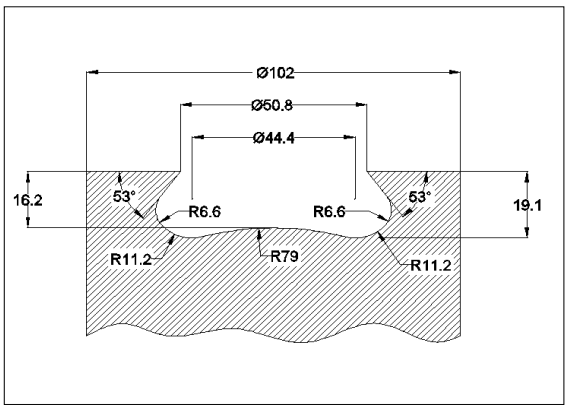

Fig. 3 Model -C: View of combustion chamber

2.1. NUMERICAL MESH AND TIME STEP:

The first and important task in the process of flow simulation is the creation of a computational mesh to represent the flow domain. In the present work the mesh represents a 360-degree of the combustion chamber. The physical model is discretized according to the mesh motion using the STAR-CD software. The models A, B and C consist of 89962, 91021 and 93709 finite volume cells respectively. A hexahedral structured mesh is used in the analysis. A time step of Δt = 0.1e-03 sec is used throughout the present study. The computational meshes are shown in Figs. 4-6.

Fig.4 Grid used for the closed model A

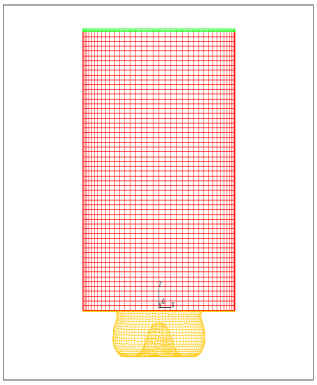

Fig. 5 Grid used for the closed cycle for model B

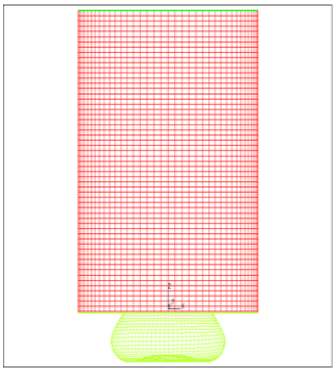

Fig. 6 Grid used for the cycle for closed cycle for model C

2.2. FLUID PROPERTIES

Table 2 In-Cylinder Air Properties

Property	**During Flow**
Density	f (T, P)
Viscosity	Constant ($1.81x10^{-5}$ Kg/ms)
Specific heat	Polynomial (1006 J/kg k)
Conductivity	Constant (0.02627 W/m K)

2.3. INITIAL AND BOUNDARY CONDITIONS

2.3.1. INITIAL CONDITIONS

Table 3. Initial conditions of air are given in the Table3

Working medium	**Pressure (bar)**	**Temperature (K)**
Air	1.00	303

2.3.2. BOUNDARY CONDITIONS

In the present computational analysis wall boundary conditions are used and the boundary regions are mentioned below

2.3.3. No-Slip wall B.C

No-slip boundary condition is provided at all the wall boundaries like cylinder head, cylinder liner and piston bowl bottom.

III. RESULTS AND DISCUSSION

3.1 MOTORING CASE RESULTS

The pollutant formation process in diesel engines are intrinsically local phenomena, most experimental and computational investigations of combustion and emission production depends upon comparison of cylinder averaged and global quantities. The measured quantities, which are related to emissions in diesel engines are average cylinder air temperature, pressure etc. In this section the motoring case results are discussed.

CFD simulations in-cylinder air motion give 3-D distribution of different quantities of interest like velocities, pressure, turbulent kinetic energy (TKE), etc. study of this results leads to clear understanding of effect of any change made to the geometry of the combustion chamber on flow and turbulence. A convention of treating the TDC as 180˚ CA is followed in figures and discussion. Swirl number and turbulent kinetic energy are identified as important with regard to in-cylinder air motion of DI diesel engine. In the present study full cylinder mesh has been used for the calculations of compression stroke.

1.1.1. COMPARISON OF SWIRL RATIO FOR MODEL A, MODEL B & MODEL

Compression and expansion strokes have been simulated for these combustion chambers. The end of suction results is used as initial condition, which is taken from Prasad (2005). Variation of mass averaged swirl number during the closed valve part of the cycle is shown in Fig. 7.

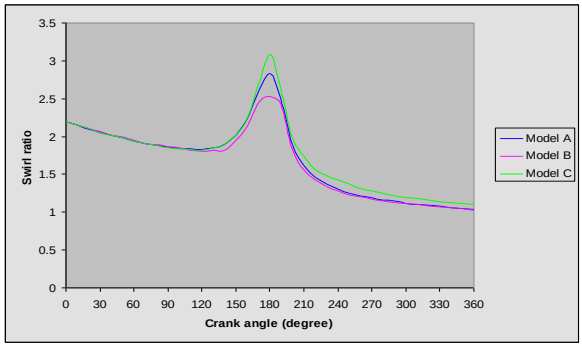

During initial part of compression there is no difference in swirl number of Model A and Model B. With regard to mixing and combustion, the swirl number from 120˚ CA to 210˚ CA is important period. But the swirl levels in cylinder with Model C are much higher than that of Model A and Model B. The peak value of swirl is about 20% higher than that of the Model A. The main reason for higher swirl number for Model C is much deeper penetration of squish flow towards the cylinder axis.

Fig.7 Average swirl number during compression and expansion

3.1.2. COMPARISON OF VELOCITY FOR MODEL A AND MODEL B

Three dimensional velocity field results, around TDC of compression, of both the geometries are considered here to investigate the possible causes of lower intensification of swirl number in Model B combustion chamber. Observing Figure 8 and 9, it can be seen that the radii of the higher velocity regions in Model A and Model B geometries is almost same.

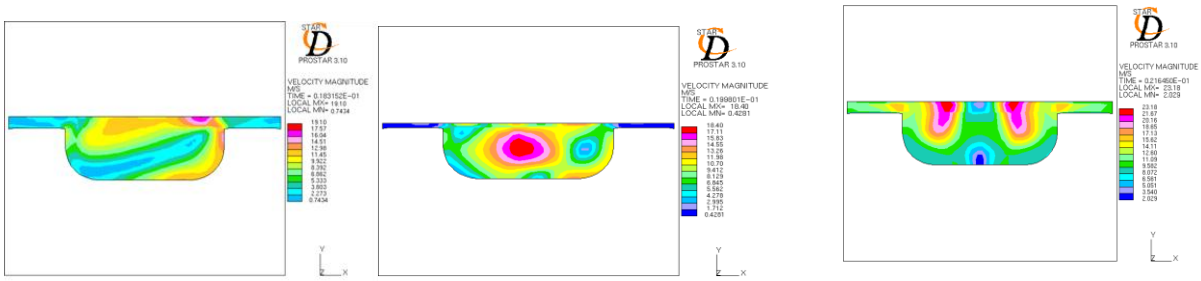

Fig.8 (a) 15 □ CA BTDC Fig.8 (b) At TDC Fig.8(c) 15 □ CA ATDC

Fig.8 Distribution of velocity in a plane passing through the Cylinder axis for Model A in x-y plane.

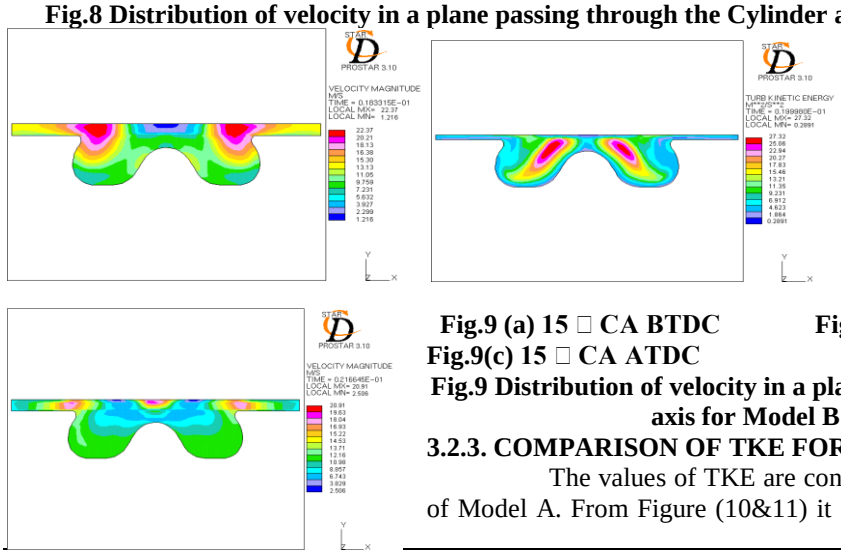

Fig.9 (a) 15 □ CA BTDC Fig.9 (b) At TDC Fig.9(c) 15 □ CA ATDC

Fig.9 Distribution of velocity in a plane passing through the cylinder axis for Model B in x-y plane.

3.2.3. COMPARISON OF TKE FOR MODEL A AND MODEL B

The values of TKE are consistently less in Model B than that of Model A. From Figure (10&11) it can be noted that, in Model B the

area of higher turbulence is less than that of Baseline. Once again the central projection is damping out the turbulence in the central part of model. During reverse squish (15° CA) the peak TKE Value is also less in Model B. The cause for this may be the jet like flow occurring across the sharp bowl edge in case of Baseline model. In Model B the bowl edge is rounded and the flow across the edge is weaker as seen in Figure (10 & 11) (At 15˚ CA).

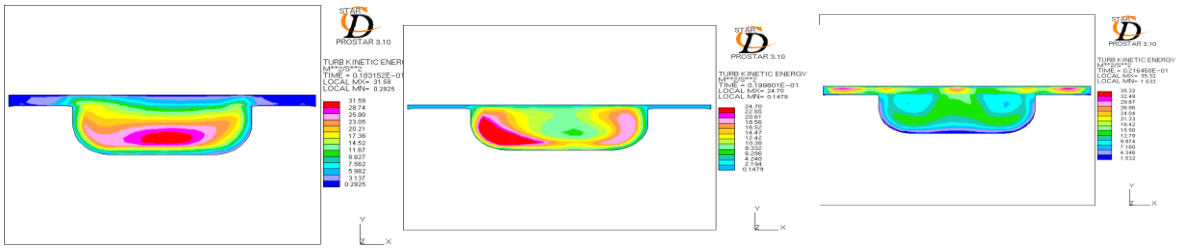

Fig.10 (a)15 □ CABTDC Fig.10 (b) At TDC Fig.10 (c) 15 □ CA ATDC
Fig.10 Distribution of TKE in a plane passing through the Cylinder axis for Model A in x-y plane.

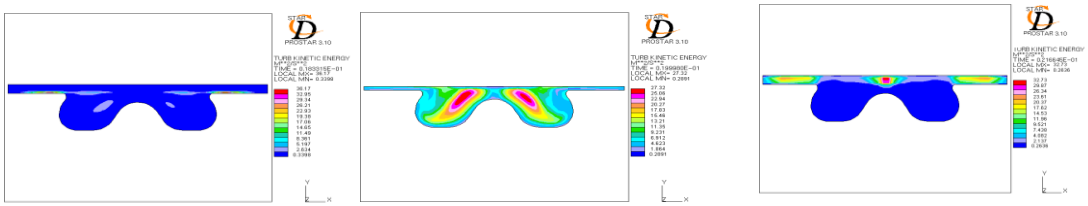

Fig.11 (a) 15 □ CA BTDC Fig.11 (b) At TDC Fig.11 (c) 15 □ CA ATDC
Fig.11 Distribution of TKE in a plane passing through the Cylinder axis for Model B in x-y plane.

3.2.4. COMPARISON OF TKE AND VELOCITY FOR MODEL A AND MODEL C

Local distributions of velocity and TKE in the bowl geometry Model C are shown in Figure (12 & 13), when compared to Model A, in Model C the velocities and TKE values are much higher. Squish flow is also penetrating much deeper towards the axis of the cylinder, which is the main reason for higher swirl intensification. During reverse squish (At 15% CA), as the sharp edge is maintained, stronger reverse-squish and very high TKE value are observed near the bowl lip. The main reasons for best performance of Model C were absence of central projection and larger re-entrant bowl with sharp bowl edge.

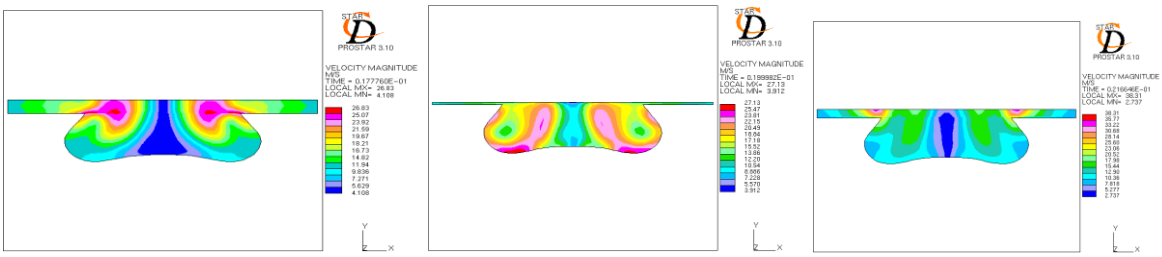

Fig.12 (a) 15 □ CA BTDC Fig.12 (b) At TDC Fig.12 (c) 15 □ CA ATDC
Fig.12 Distribution of velocity in a plane passing through the cylinder axis for Model C in x-y plane

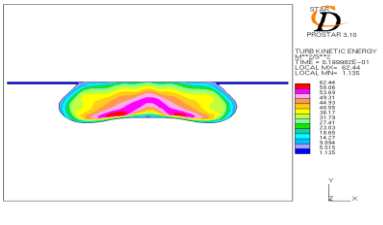
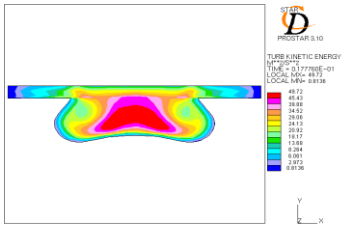
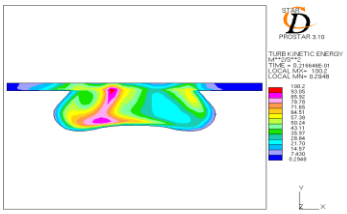

Fig.13 (a) 15 □ CA BTDC **Fig.13 (b) At TDC** **Fig.13 (c) 15 □ CA ATDC**

Fig.13 Distribution of TKE in a plane passing through the cylinder axis for Model C in x-y plane.

3.2.5. CYLINDER PRESSURE AND TEMPERATURE

From the motored condition results it is observed that the maximum average cylinder temperature and pressure is attained near TDC and the corresponding values are given in table 4. It can be seen that peak pressure is on the higher side. The Figures 14 to 19 shows the pressure and temperature distribution across the cylinder at TDC for three model. The peak pressure and temperature values are obtained near by the cylinder walls. This is because of the fact that, the air is confined to smaller area near the cylinder walls, resulting in it being highly compressed.

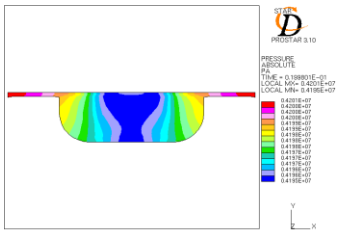
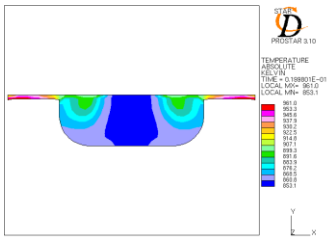
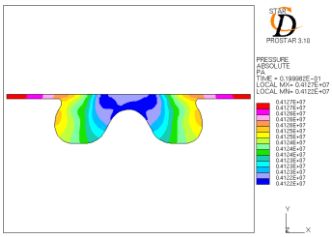

Fig.14 Pr. Distribution at TDC for Model A **Fig.15 Temp. Distribution at TDC for Model A** **Fig.16 pr. Distribution at TDC for Model B**

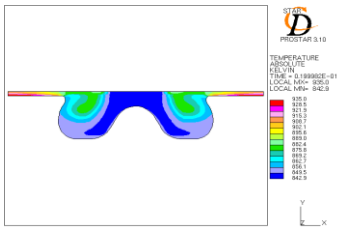
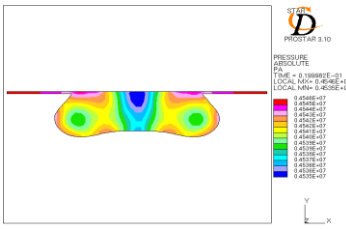
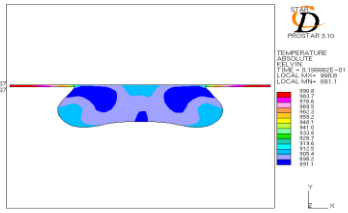

Fig.16 Temp. Distribution at TDC for Model B **Fig.17 Pr. Distribution at TDC for Model C** **Fig.18 pr. Distribution at TDC for Model C**

COMPARISON OF SWIRL RATIO

The maximum swirl ratio for the three bowls is shown below

S.NO	MODELS	MAXIMUM SWIRL RATIO
1	Model-A	2.78
2	Model-B	2.52
3	Model-C	3.1

The Model C having the maximum swirl ratio when compared to other models**.** Sharp piston bowl edge of the Model C helps in increasing turbulence during squish and reverse squish process.

The variation of pressure in the fluid domain as the piston completes the compression and expansion strokes is given in the Figure 20

From the above figure 20, it is clear that the model C has higher pressure at TDC of compression stroke than other models for motoring case.

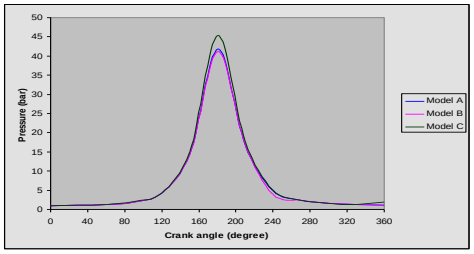

Fig.20 Pressure versus Crank angle diagram for motoring case

3.1.8. T- □ CURVE

The variation of temperature in the fluid domain as the piston completes the compression and expansion strokes is given in the figure 21. it is clear that the model C has higher temperature at TDC of compression stroke than other models for motoring case.

$$\frac{P_2}{P_1} = \left(\frac{V_1}{V_2}\right)^{\gamma} \qquad 3.1$$

$$\frac{T_2}{T_1} = \left(\frac{P_2}{P_1}\right)^{\frac{\gamma-1}{\gamma}} \qquad 3.2 \quad \text{Where } \gamma = 1.4$$

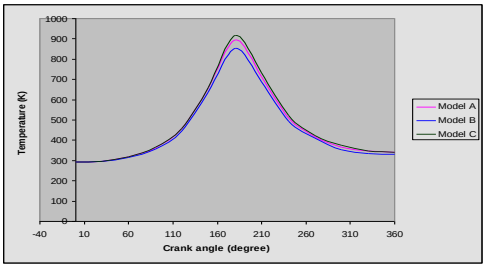

Fig.21 Temperature vs. Crank Angle for Motored Case

The Model C has the maximum temp. and pressure when compared to Model A and Model B. The quantitative agreement of the simulated and calculated values validates the flow simulation carried out. The variation between the theoretical and experiment values is less than 5 %.

Table.5 Comparisons of Simulated and Calculated Peak Temp. and Pressure Values

Variable	Simulated	Calculated
Peak temperature (K) for model A	895.63	926
Peak temperature (K) for model B	852.47	926
Peak temperature (K) for model C	918.00	926
Peak pressure (bar) for Model A	46.949	49.78
Peak pressure (bar) for Model B	46.244	49.78
Peak pressure (bar) for Model C	47.424	49.78

IV. CONCLUSION

This study shows that the swirl number and turbulence intensification near TDC of compression for Model B was found to be worse than Model A and Model C. The central projection was found to be obstructing the penetration of squish flow and increasing the skin friction. Also the re-entrancy was found to be inefficient. Sharp piston bowl edge found to be helping in increasing turbulence during reverse squish process. Around TDC of combustion, the in-cylinder flow found to be not very axisymmetric and better estimation of in-cylinder flow field and TKE levels of Model C are much higher than Model A and Model B. Squish and reverse squish motions are also observed to be strong in Model C.

REFERENCES

[1]. Arturo de Risi, Teresa Donateo, Domenico Laforgia,"Optimization of the Combustion Chamber of Direct Injection Diesel Engines", SAE 2003-01-1064.
[2]. Bianchi, G.M., Pelloni, P., Corcine, F.E. Mattarelli, E.Luppino, Bertoni. F, "Numerical Study of the Combustion Chamber Shape for Common Rail H.S.D.I Diesel Engines", SAE 2000-01-1179.
[3]. Corcione. F. E, Annunziata Fusca, and Gerardo Valentino, "Numerical and Experimental Analysis of Diesel Air Fuel Mixing", SAE 931948.
[4]. Herbert Schapertons, Fred Thiele," Three Dimensional Computations for Flow Fields in D I Piston Bowls", SAE 860463.
[5]. Ikegami. M, Fukuda. M, Yoshihara. Y and Kaneko. J, "Combustion Chamber Shape and Pressurized Injection in High- Speed Direct –Injection Diesel Engines", SAE 900440.
[6]. John B. Heywood, "Internal Combustion Engine Fundamentals"
[7]. Ogawa. H, Matsui. Y, Kimura. S, Kawashima. J, "Three Dimensional Computation of the Effects of the Swirl Ratio in Direct- Injection Diesel Engines on NOx and Soot emissions", SAE 961125.
[8]. Prasad. B.V.V.S, Ravikrishna .R.V, "CFD Simulation of in-cylinder air flow in a D I Diesel Engine – Effect of Combustion Chamber Geometry", proceedings of the 19th conference on IV Engines and Combustion.
[9]. Payri. F, Benajes .J, Margot .X, Gil. A, "CFD Modeling of the In-Cylinder Flow in Direct –Injection Diesel Engines", Computers and Fluids 33 (2004) 995-1021.
[10]. Paul. B and Ganesan. V, "CFD Analysis of the Effect of Port Configurations on Air Motion Inside the Cylinder of a DI Diesel Engine" Proceedings of the 19th Conference on I C Engines and Combustion., 2005
[11]. Ramalingam. K. K, " Internal Combustion Engines – Theory and Practice "
[12]. Wakisaka.T, Shimamoto.Y and Isshiki .Y,"Three dimensional numerical analysis of in- cylinder flows in reciprocating engines", SAE 860464.
[13]. Zhang. L, Ueda .T, Takatsuki .K, "A Study of the effects of Chamber Geometrics on Flame Behavior in DI diesel Engine", SAE 95255, 1995.